A Visible Light–Driven Artificial Molecular Switch Actuated by Radical–Radical and Donor–Acceptor Interactions

ARTICLE *in* THE JOURNAL OF PHYSICAL CHEMISTRY A · MAY 2015

Impact Factor: 2.69 · DOI: 10.1021/acs.jpca.5b04570

9 AUTHORS, INCLUDING:

Zhichang Liu
Northwestern University
32 PUBLICATIONS **423** CITATIONS
SEE PROFILE

Dennis D Cao
Macalester College
30 PUBLICATIONS **666** CITATIONS
SEE PROFILE

Yuping Wang
Northwestern University
6 PUBLICATIONS **15** CITATIONS
SEE PROFILE

Chuyang Cheng
Northwestern University
22 PUBLICATIONS **196** CITATIONS
SEE PROFILE

THE JOURNAL OF PHYSICAL CHEMISTRY A

Article

pubs.acs.org/JPCA

Visible Light-Driven Artificial Molecular Switch Actuated by Radical–Radical and Donor–Acceptor Interactions

Junling Sun,[†] Yilei Wu,[†,‡] Zhichang Liu,[†] Dennis Cao,[†] Yuping Wang,[†] Chuyang Cheng,[†] Dongyang Chen,[†] Michael R. Wasielewski,*[,†,‡] and J. Fraser Stoddart*[,†]

[†]Department of Chemistry, Northwestern University, 2145 Sheridan Road, Evanston, Illinois 60208-3113, United States

[‡]Argonne-Northwestern Solar Energy Research (ANSER) Center, Northwestern University, 2145 Sheridan Road, Evanston, Illinois 60208-3113, United States

Supporting Information

ABSTRACT: We describe a visible light-driven switchable [2]catenane, composed of a $Ru(bpy)_3^{2+}$ tethered cyclobis(paraquat-*p*-phenylene) ($CBPQT^{4+}$) ring that is interlocked mechanically with a macrocyclic polyether consisting of electron-rich 1,5-dioxynaphthalene (DNP) and electron-deficient 4,4′-bipyridinium ($BIPY^{2+}$) units. In the oxidized state, the $CBPQT^{4+}$ ring encircles the DNP recognition site as a consequence of favorable donor–acceptor interactions. In the presence of an excess of triethanolamine (TEOA), visible light irradiation reduces the $BIPY^{2+}$ units to $BIPY^{(\bullet+)}$ radical cations under the influence of the photosensitizer $Ru(bpy)_3^{2+}$, resulting in the movement of the $CBPQT^{2(\bullet+)}$ ring from the DNP to the $BIPY^{(\bullet+)}$ recognition site as a consequence of the formation of the more energetically favorable trisradical complex, $BIPY^{(\bullet+)} \subset CBPQT^{2(\bullet+)}$. Upon introducing O_2 in the dark, the $BIPY^{(\bullet+)}$ radical cations are oxidized back to $BIPY^{2+}$ dications, leading to the reinstatement of the $CBPQT^{4+}$ ring encircled around the DNP recognition site. Employing this strategy of redox control, we have demonstrated a prototypical molecular switch that can be manipulated photochemically and chemically by sequential reduction and oxidation.

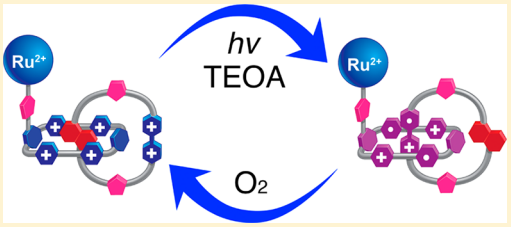

INTRODUCTION

In the macroscopic world, machines can do work by performing energy-driven predetermined movements. Likewise, at nanoscopic levels, so-called molecular machines are capable of carrying out net nuclear movements to fulfill specific functions with the input of energy from external stimuli. Molecular machines, which are essential for controlling and maintaining a variety of biological functions, exist[1] widely in nature. A classical example[2−5] is ATP synthase. Proton flux through cell membranes drives the rotation of the F_o domain of the ATP synthase, which in turn initiates the rotation of the γ-subunit in the F_1 domain. Subsequently, the rotation of the γ-subunit can change sequentially the conformations of the three alternatively arranged β-subunits, which are responsible for the catalytic production of ATP molecules. Each 360° rotation of the γ-subunit produces three ATP molecules. Other representative biological molecular machines include myosins,[6,7] kinesins,[8] and bacterial flagella.[9]

Inspired by these elegant and sophisticated motors in the biological world, chemists have set about designing and synthesizing[10−20] various primitive nanoscale artificial molecular machines, among which those derived from the mechanically interlocked molecules[21−29] or MIMs for short—namely, bistable rotaxanes and bistable catenanes—have emerged as a class of very important frontrunners on account of their highly controllable mechanical motions in response to external stimuli. They have shown considerable potential for applications in the realms of nanoelectronics,[30−34] drug delivery,[35,36] and more recently, catalysis.[37−42] Bistable rotaxanes, molecules having one ring encircling a linear rod component containing two different recognition sites and terminated by bulky stoppers to prevent the ring from dethreading, are capable of undergoing switching motions when addressed by external stimuli. Bistable catenanes are molecular structures containing two mechanically interlocked rings, which are capable of undergoing relative circumrotational movements between different recognition sites when addressed chemically, electrochemically, or photochemically. All these external stimuli-induced motions are achieved by manipulating the binding affinities of rings for a couple of different recognition sites.

Over the past few decades, investigations of the pros and cons of various external stimuli have been the subject of intense research efforts. Chemical,[43−46] electrochemical,[47−49] optical stimuli,[50−57] and others have been developed and employed to induce relative mechanical motions in MIMs. Of these, visible light is considered to be a desirable stimulus because it is an easily accessible and clean energy source. So far, however, the visible light-driven switchable [2]catenanes have not been fully explored.

Recently, we reported[58] two bistable [2]catenanes sharing a similar structure in which a cyclobis(paraquat-*p*-phenylene) ($CBPQT^{4+}$) ring is interlocked mechanically with macrocyclic

Received: May 15, 2015

DOI: 10.1021/acs.jpca.5b04570
J. Phys. Chem. A XXXX, XXX, XXX−XXX

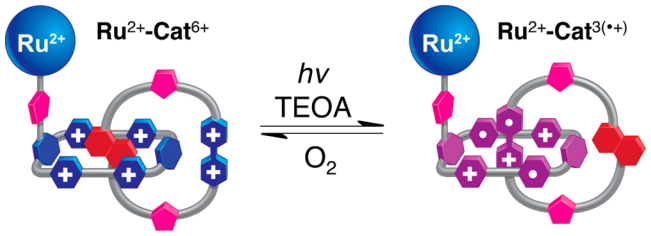

Figure 1. Representation of the switching between Ru^{2+}-Cat^{6+} and Ru^{2+}-$Cat^{3(•+)}$ driven by visible light and oxidation.

polyethers (MC^{2+}) consisting of a 4,4′-bipyridinium ($BIPY^{2+}$) unit and a 1,5-dioxynaphthalene (DNP) unit. Both of them exhibit electrochemically switchable behavior in which the $CBPQT^{4+}$ ring migrates between the DNP (oxidized state) and the $BIPY^{(•+)}$ (reduced state) recognition site, dependent on donor–acceptor[59] and radical–radical interactions,[60−63] respectively. In both states, the switching takes place quantitatively. To enable these electrochemically switchable MIMs to be responsive to visible light stimulus, we decided to attach a $Ru(bpy)_3^{2+}$ complex to one of these bistable [2]catenanes. The properties of this photoactive switchable [2]catenane have been investigated by UV–vis–NIR, ^1H NMR, and electron paramagnetic resonance (EPR) spectroscopies. Fully reversible switching, driven sequentially by visible light and O_2, has been demonstrated. Even after recycling five times, the molecular switch continues to perform and no significant decomposition of the bistable [2]catenane has been observed.

The switching mechanism of the photoactive bistable [2]catenane is illustrated in Figure 1. In its oxidized state, the $CBPQT^{4+}$ ring encircles the DNP recognition site because of donor–acceptor interactions. When the catenane is irradiated by visible light in the presence of a sacrificial electron donor, the $Ru(bpy)_3^{2+}$ unit brings about the photoreduction of $BIPY^{2+}$ units in both the MC^{2+} ring and the $CBPQT^{4+}$ ring, leading to the formation of a thermodynamically stable trisradical co-conformation[63] $BIPY^{(•+)} \subset CBPQT^{2(•+)}$, which causes the movement of the $CBPQT^{2(•+)}$ ring from the DNP to the $BIPY^{(•+)}$ recognition site. Subsequently, by bubbling air into the system, all the $BIPY^{(•+)}$ units are oxidized back to $BIPY^{2+}$ dications. Consequently, the $CBPQT^{4+}$ ring returns to encircling the original DNP recognition site, thus completing the switching cycle, which has been followed by (i) UV–vis–NIR absorption spectroscopy, (ii) steady-state and time-resolve photoluminescence spectroscopy, and (iii) femtosecond transient absorption (fsTA) spectroscopy, in addition to (iv) ^1H NMR and (v) EPR spectroscopies. In this mechanically interlocked system, the switching process is driven by noncovalent interactions in both states, in contradistinction to the previous metal-coordination driven examples.

RESULTS AND DISCUSSION

The bench-stable $Ru(bpy)_3^{2+}$ complex has long been known to be[64−67] an excellent photocatalyst. It enables efficient harvesting of visible light to form a long-lived triplet excited state (^3MLCT) that becomes[67] an effective reductant for viologen derivatives. We expected that by grafting the $Ru(bpy)_3^{2+}$ complex onto one of aforementioned bistable [2]catenanes, we might be able to fabricate a visible light-responsive molecular switch. The synthesis (Scheme 1) of the photoactive [2]catenane **Ru-Cat**·$8PF_6$ begins with the preparation of a known $Ru(bpy)_3^{2+}$ complex[68] **1**·$2PF_6$ and a monoazide substituted $CBPQT^{4+}$ derivative[69] **2**·$4PF_6$. A subsequent Cu(I)-catalyzed azide–alkyne cycloaddition reaction (CuAAC) between these two precursors afforded **Ru-Box**·$6PF_6$ in 90% yield. To obtain a bistable [2]catenane, two commonly used synthetic approaches—namely, a clipping

Scheme 1. Synthesis of the Photoactive Bistable [2]Catenane Ru-Cat·$8PF_6$

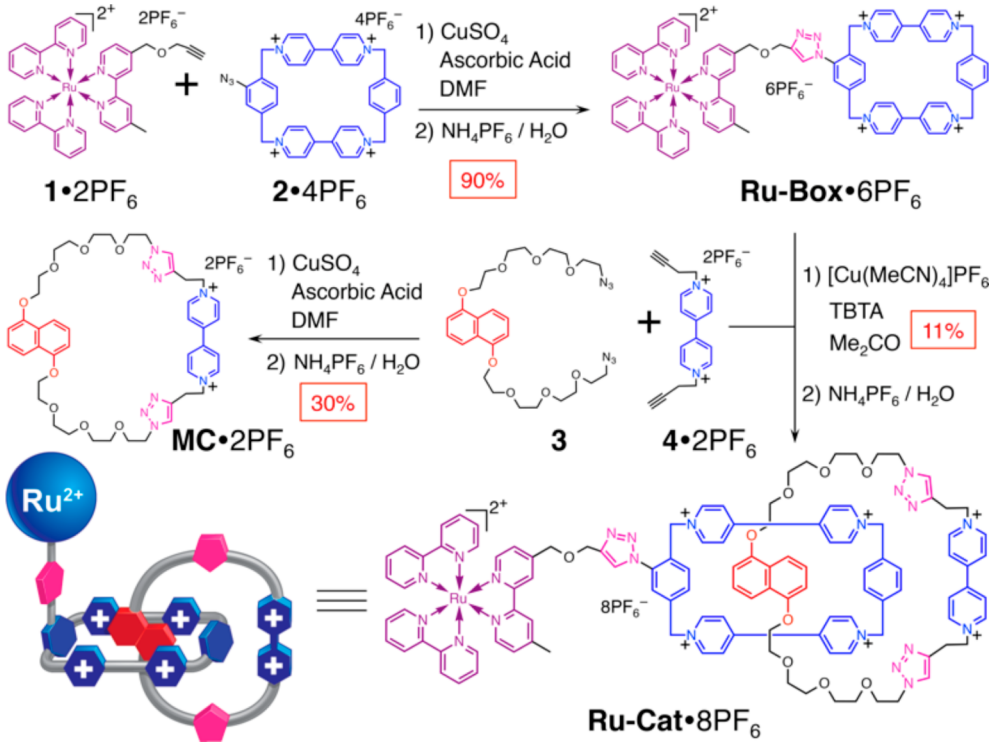

DOI: 10.1021/acs.jpca.5b04570
J. Phys. Chem. A XXXX, XXX, XXX−XXX

approach[70] or a threading-followed-by-cyclization approach[71]—could be utilized potentially. A previous report[58] had revealed, however, that the clipping approach, which requires the DNP unit to act as a template for CBPQT^{4+} ring formation, is not practical because of strong intramolecular donor−acceptor interactions between DNP and BIPY^{2+} units within macrocycles such as **MC**$^{2+}$, hence preventing the DNP unit from templating the formation of the CBPQT^{4+} ring. Thus, a threading-followed-by-cyclization approach, involving first of all the formation of the complex **3** ⊂ **Ru**$^{2+}$**-Box**$^{4+}$ followed by catenation employing a CuAAC reaction, was pursued. Before performing the reaction, the formation of the complex between **Ru**$^{2+}$**-Box**$^{4+}$ and **3** was investigated by ^{1}H NMR spectroscopy. The spectrum (Figure S6, Supporting Information) of an equimolar mixture of **Ru**$^{2+}$**-Box**$^{4+}$ and **3** recorded at 243 K reveals significant upfield shifts of DNP proton resonances, $H_{2/6}$, $H_{3/7}$, and $H_{4/8}$, by 4.31, 1.08, and 0.48 ppm, respectively, strongly supporting the formation of the **3** ⊂ **Ru**$^{2+}$**-Box**$^{4+}$ complex. At higher temperatures, 293 K for example, the spectrum displays extensive broadening of the proton resonances for the CBPQT^{4+} ring as well as for **3**, an observation that indicates the exchange rate between the complexed and free **3** is intermediate in speed on the ^{1}H NMR time scale. In the event, the CuAAC reaction between the preformed complex **3** ⊂ **Ru-Box**·6PF$_6$ and **4**·2PF$_6$ afforded **Ru-Cat**·8PF$_6$ in 11% yield. The low yield can be attributed to the energetically unfavorable transition state arising from Coulombic repulsion between the BIPY^{2+} unit and the CBPQT^{4+} ring. The yield is very similar to that recorded for a related [2]catenane,[58] suggesting that the tethered Ru(bpy)$_3^{2+}$ unit has very little influence, if at all, on the binding properties of the CBPQT^{4+} ring and, accordingly, the catenation efficiency. **Ru-Cat**·8PF$_6$ was characterized in solution by ^{1}H, ^{13}C, ^{1}H−^{1}H gDQCOSY, and DOSY NMR spectroscopies as well as by high-resolution mass spectrometry (HRMS). See Supporting Information for the full characterization data.

The ^{1}H DOSY NMR spectrum (Figure S5, Supporting Information) of **Ru**$^{2+}$**-Cat**$^{6+}$ recorded in CD$_3$CN reveals that its two components, namely, Ru^{2+}-Box^{4+} and MC^{2+}, diffuse at the same rate of 1.35×10^{-5} cm^2 s^{-1}, an observation supporting the fact that the two components are mutually interlocked. The proton resonances in ^{1}H NMR spectra of (a) **MC**$^{2+}$, (b) **Ru**$^{2+}$**-Cat**$^{6+}$, and (c) **Ru**$^{2+}$**-Box**$^{4+}$ in CD$_3$CN at 343 K are compared in Figure 2. The resonances for the DNP protons, $H_{2/6}$, $H_{3/7}$, and $H_{4/8}$, in **Ru**$^{2+}$**-Cat**$^{6+}$ are shifted dramatically upfield by 0.44, 1.12, and 4.37 ppm, respectively, indicating that the CBPQT^{4+} ring encircles the DNP unit in the oxidized state. Meanwhile, downfield shifts in the proton resonances ($H_{\alpha'}$ and $H_{\beta'}$) associated with the BIPY^{2+} unit of the MC^{2+} ring are observed. It stands to reason that the BIPY^{2+} unit is located in the deshielding region of the CBPQT^{4+} ring so as to minimize the Coulombic repulsion, a conclusion in a good agreement with the previous observations.[58] On the contrary, when the proton resonances for **Ru**$^{2+}$**-Cat**$^{6+}$ were compared with those for **Ru**$^{2+}$**-Box**$^{4+}$, the chemical shifts for the Ru(bpy)$_3^{2+}$ proton resonances were found to be almost the same in both molecules, indicating a lack of interactions between the Ru(bpy)$_3^{2+}$ unit and either the CBPQT^{4+} or the MC^{2+} ring.

VT ^{1}H NMR spectroscopy was employed to probe the co-conformational dynamics of **Ru**$^{2+}$**-Box**$^{4+}$ and **Ru**$^{2+}$**-Cat**$^{6+}$. In the case of **Ru**$^{2+}$**-Box**$^{4+}$, only temperature-induced proton resonance shifts were observed (Figure S7, Supporting Information) over the range 243−299 K. The absence of coalescences

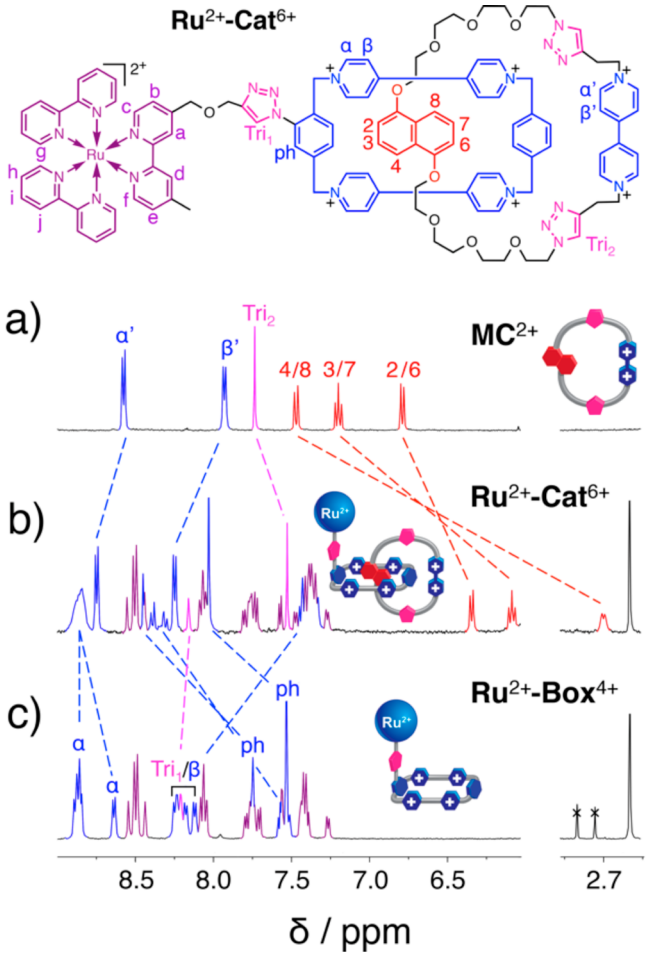

Figure 2. Comparison of the partial ^{1}H NMR spectra (500 MHz, CD$_3$CN, 343 K) of (a) **MC**$^{2+}$, (b) **Ru**$^{2+}$**-Cat**$^{6+}$, and (c) **Ru**$^{2+}$**-Box**$^{4+}$. Assignment of proton resonances was made with the assistance of ^{1}H−^{1}H gDQCOSY.

suggests that the BIPY^{2+} units and phenylene groups of the CBPQT^{4+} ring rotate quickly on the ^{1}H NMR time scale throughout the entire temperature range. By contrast, ^{1}H NMR spectra (Figure 3) recorded over a temperature range of 243−343 K for **Ru**$^{2+}$**-Cat**$^{6+}$ reveal that the α, β, and phenylene proton resonances associated with the CBPQT^{4+} ring, as well as the DNP proton resonances of the MC^{2+} ring, do undergo coalescence. The coalescence temperatures (T_c), namely, 303, 263, and 283 K, for α, β, and phenylene proton resonances, respectively, are a consequence of the rotations (process I) of the BIPY^{2+} units and the phenylene groups. The exchange rate at each T_c can be calculated,[72] and thus thermodynamic parameters, $\Delta H^{\ddagger} = 4.2$ kcal mol^{-1}, $\Delta S^{\ddagger} = -39.8$ cal mol^{-1} K^{-1}, and $\Delta G^{\ddagger}(298\ \text{K}) = 16.1$ kcal mol^{-1} were obtained (Figure S8a, Supporting Information) for process I using the Eyring plot.[73] Similarly, the coalescences of the DNP proton resonances correspond to the dynamic motions (process II) of the DNP unit, which involve three steps—(i) the initial DNP unit dissociating from the CBPQT^{4+} ring, (ii) followed by a vertical flip of the unit with respect to the DNP plane, and (iii) re-entry of the DNP unit inside the CBPQT^{4+} ring. Because the T_c for all three different sets of DNP proton resonances are observed at 283 K, a further line-shape analysis[74] on $H_{2/6}$, at different temperatures, was carried out (Figure S9, Supporting Information) to obtain the thermodynamic parameters for

DOI: 10.1021/acs.jpca.5b04570
J. Phys. Chem. A XXXX, XXX, XXX−XXX

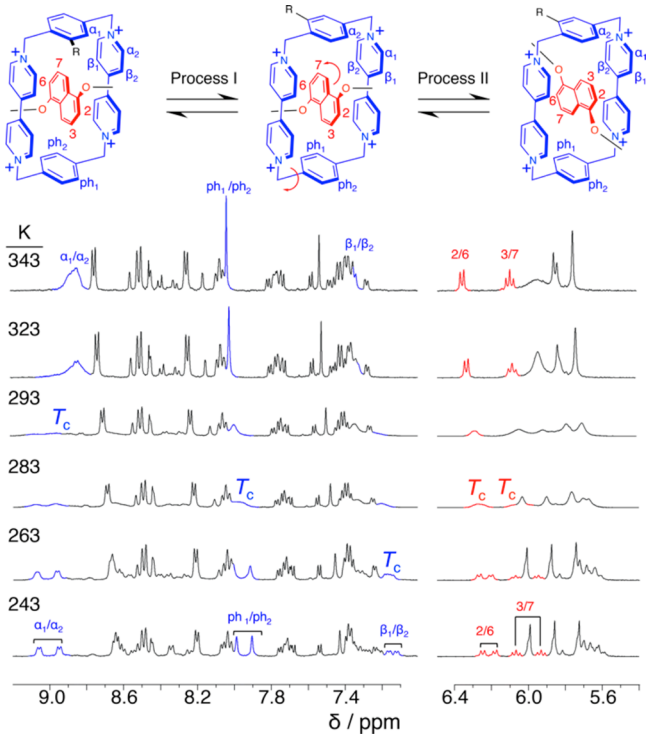

Figure 3. VT ^{1}H NMR Spectra (400 MHz, CD_3CN) of **Ru-Cat**$^{8+}$ exhibiting two dynamic processes. Proton resonances undergoing coalescence are annotated on the spectra.

process II—that is, $\Delta H^{\ddagger}$ = 5.4 kcal mol^{-1}, $\Delta S^{\ddagger}$ = −36.2 cal mol^{-1} K^{-1}, and $\Delta G^{\ddagger}$(298 K) = 14.4 kcal mol^{-1}.

Although the cyclic voltammogram (CV) of the free **MC**$^{2+}$ exhibits (Figure 4a) two reversible consecutive one-electron reductions—namely, **MC**$^{2+}$ → **MC**$^{(\bullet+)}$ at a peak potential of −424 mV and **MC**$^{(\bullet+)}$ → **MC**^{0} at −859 mV—the reduction of the free **Ru**$^{2+}$**-Box**$^{4+}$ takes place (Figure 4c) by two two-electron and one one-electron reduction processes. The first two reduction waves correspond to two-step consecutive reductions of the CBPQT^{4+} ring occurring at −344 mV (CBPQT^{4+} → CBPQT$^{2(\bullet+)}$) and −736 mV (CBPQT$^{2(\bullet+)}$ → CBPQT^{0}), respectively. The third reduction wave is a consequence[57] of the one-electron reduction [Ru(bpy)$_3^{2+}$ → Ru(bpy)$_3^{+}$] of the Ru(bpy)$_3^{2+}$ unit, occurring at −1376 mV. By way of contrast, the first reduction wave (Figure 4b) for **Ru**$^{2+}$**-Cat**$^{6+}$, which occurs at −280 mV, is a three-electron process where two electrons are transferred to the LUMOs of the two BIPY^{2+} units in the CBPQT^{4+} ring and one electron is transferred to the LUMO of the remaining BIPY^{2+} unit in the MC^{2+} ring. The single three-electron reduction gives rise to the formation of the BIPY$^{(\bullet+)}$ ⊂ CBPQT$^{2(\bullet+)}$ co-conformation. When compared with the first reduction waves for both individual components, that for **Ru-Cat**$^{8+}$ is shifted to more positive potentials as a consequence of the presence of favorable radical−radical interactions.[63] The second reduction wave, which occurs at −736 mV, can be assigned to a one-electron reduction of one of two BIPY$^{(\bullet+)}$ units in the CBPQT$^{2(\bullet+)}$ ring. The reduction of the remaining two BIPY^{2+} units takes place at −839 and −1002 mV in contrast with the previous observations[58] on trisradical complexes where the two BIPY^{2+} units are reduced simultaneously. It is not unlikely that the bulky Ru(bpy)$_3^{2+}$ unit slows down the mechanical movement of the MC^{2+} ring, thus amplifying the radical−radical pair interactions and resulting in a stepwise reduction of the last two BIPY^{2+} units. The last reduction wave observed at −1378 mV corresponds to the reduction of the Ru(bpy)$_3^{2+}$ unit. Overall, the CV measurements imply that the electrochemical reduction of **Ru**$^{2+}$**-Cat**$^{6+}$ is associated with some kind of switching process, prompting us to investigate the photoswitching behavior of this functionalized bistable [2]catenane.

A prerequisite to being able to trigger the switching of **Ru**$^{2+}$**-Cat**$^{6+}$ using visible light is the efficient electron transfer from the ^{3}MLCT state of the Ru(bpy)$_3^{2+}$ unit to all of the three other BIPY^{2+} units. To probe the electron-transfer process, we measured (Figure 5) the photoluminescence of **Ru**$^{2+}$**-Cat**$^{6+}$ in a deaerated MeCN solution alongside two reference compounds—namely, **1**$^{2+}$ and **Ru**$^{2+}$**-Box**$^{4+}$. Although **1**$^{2+}$ exhibits (Figure 5a) a strong emission band (Φ_{em} = 8.2%) centered on 610 nm as expected on the basis of a previous report,[75] the emission of **Ru**$^{2+}$**-Box**$^{4+}$ is quenched quantitatively (Φ_{em} = 0.04%), indicating an efficient photoinduced electron transfer (Φ_{PET} = 99.5%) from the emissive ^{3}MLCT state of the Ru(bpy)$_3^{2+}$ unit to the BIPY^{2+} units. Quantitative quenching (Φ_{em} = 0.09%) was also observed in the case of **Ru**$^{2+}$**-Cat**$^{6+}$, indicating that the efficiency of the electron-transfer process (Φ_{PET} = 98.9%) is changed only marginally in the catenated compound. The efficient electron transfer within **Ru**$^{2+}$**-Cat**$^{6+}$ was confirmed (Figure 5b) by time-resolved photoluminescence experiments. The emission lifetime of **1**$^{2+}$ was found to be 956 ns, in good agreement[76] with the reported value. In contrast, the emission lifetimes of **Ru**$^{2+}$**-Box**$^{4+}$ and **Ru**$^{2+}$**-Cat**$^{6+}$ are only 3.0 and 3.6 ns, respectively, implying that the emissive

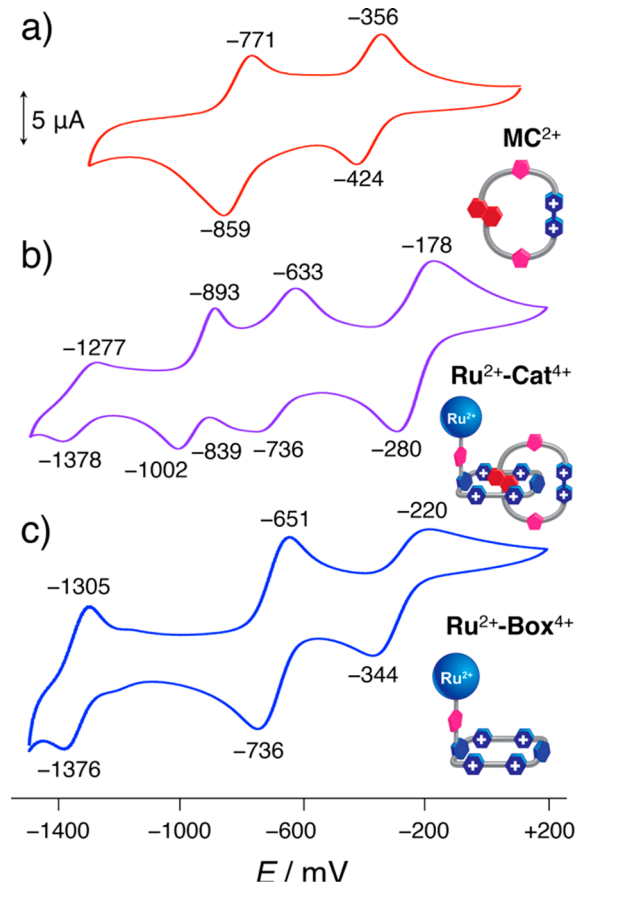

Figure 4. Comparison of CVs (MeCN, 0.1 M $TBAPF_6$, 200 mV·s^{-1}) of 1 mM solutions of (a) **MC**$^{2+}$, (b) **Ru**$^{2+}$**-Cat**$^{6+}$, and (c) **Ru**$^{2+}$**-Box**$^{4+}$.

DOI: 10.1021/acs.jpca.5b04570
J. Phys. Chem. A XXXX, XXX, XXX−XXX

^{3}MLCT state of the $Ru(bpy)_3^{2+}$ unit relaxes more quickly by transferring an electron to the $BIPY^{2+}$ acceptor.

The dynamics associated with the photoinduced process was also investigated by performing fsTA experiments (Figures 6 and S10, Supporting Information). Following excitation of the $Ru(bpy)_3^{2+}$ chromophore in **Ru^{2+}-Cat^{6+}** and **Ru^{2+}-Box^{4+}** with a 415 nm, 150 fs pulse, the initial transient absorption spectra are characterized by (i) a positive absorption feature around 605 nm and by (ii) a negative absorption feature at 450 nm, which can be assigned to the $BIPY^{(\bullet+)}$ radical cations and the bleaching of ground-state of the $Ru(bpy)_3^{2+}$ unit, respectively. The absorptions of reduced $BIPY^{(\bullet+)}$ units rise in $\tau = 1.1 \pm 0.02$ ns for **Ru^{2+}-Box^{4+}** and 1.7 ± 0.1 ns for **Ru^{2+}-Cat^{6+}** (fit at λ_{max} = 605 nm, Figure S11, Supporting Information), in good agreement with the decay constants measured by photoluminescence experiments and decay in 7.9 ± 0.1 ns for **Ru^{2+}-Box^{4+}** and 10.0 ± 0.1 ns for **Ru^{2+}-Cat^{6+}**. The transient absorption spectra of **1^{2+}** are characterized by a long-lived ^{3}MLCT state.

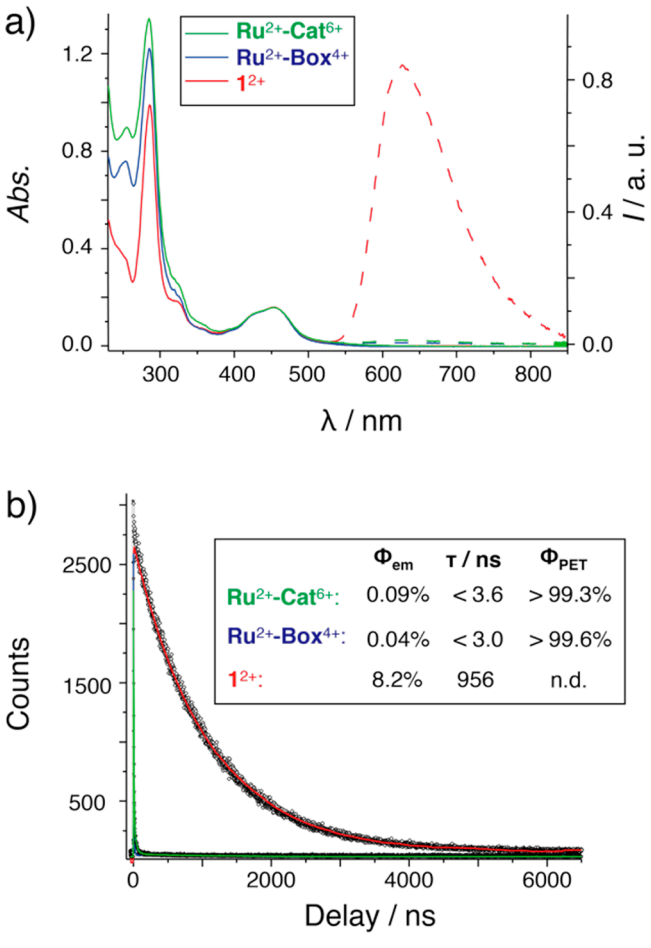

Figure 5. (a) Steady-state photoluminescence spectra (MeCN, 298 K, argon, λ_{exc} = 450 nm) of 10 μM solutions of **1^{2+}**, **Ru^{2+}-Box^{4+}**, and **Ru^{2+}-Cat^{6+}** showing quantitative quenching of luminescence from ^{3}MLCT state of the $Ru(bpy)^{2+}$ unit in both **Ru^{2+}-Box^{4+}** and **Ru^{2+}-Cat^{6+}**. (b) The time-resolved photoluminescence decay traces recorded (MeCN, 298 K, argon, λ_{exc} = 450 nm) for 10 μM solutions of **1^{2+}**, **Ru^{2+}-Box^{4+}**, and **Ru^{2+}-Cat^{6+}** showing dramatic decrease in lifetime of ^{3}MLCT state of the $Ru(bpy)^{2+}$ unit in both **Ru^{2+}-Box^{4+}** and **Ru^{2+}-Cat^{6+}**.

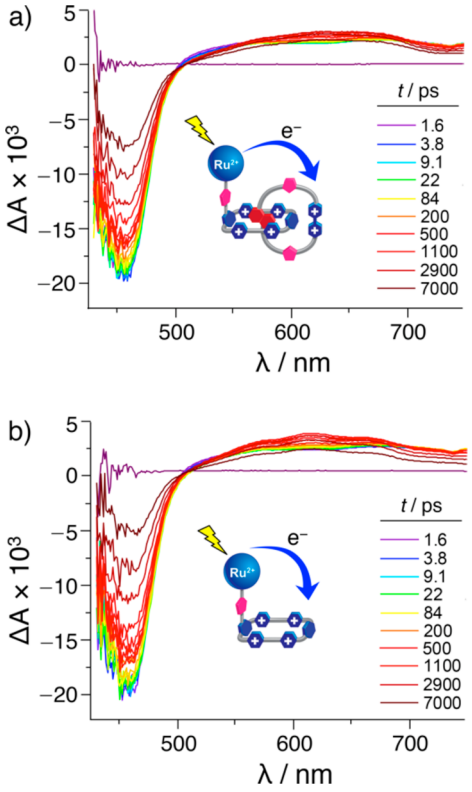

Figure 6. Stacked fsTA spectra recorded for MeCN solutions of (a) **Ru^{2+}-Cat^{6+}** and (b) **Ru^{2+}-Box^{4+}**, exciting at λ_{exc} = 415 nm (150 fs pulse), highlighting the characteristic $BIPY^{\bullet+}$ absorption centered on 605 nm.

Generally speaking, the back-electron transfer from the reduced $BIPY^{(\bullet+)}$ unit to the oxidized $Ru(bpy)_3^{3+}$ unit is very fast in the absence of sacrificial electron donors.[77] Therefore, triethanolamine[78] (TEOA), which is among the most frequently used sacrificial electron donors, was added to the system to suppress the back-electron transfer.

First of all, we investigated the photoreduction behavior of **Ru^{2+}-Box^{4+}** by UV−vis−NIR spectroscopy. In the oxidized state, the spectrum (Figure 7a) exhibits a characteristic metal-to-ligand charge-transfer (MLCT) absorption band centered around 450 nm and a ligand-centered (LC) absorption band in the UV region associated with the $Ru(bpy)_3^{2+}$ unit as well as a characteristic absorption band centered on 255 nm corresponding to the $\pi-\pi^*$ transition of $BIPY^{2+}$ units. **Ru^{2+}-Box^{4+}**, in the presence of TEOA, was irradiated in a deaerated MeCN solution at 450 nm by employing a laser source, which was intermittently monitored by UV−vis−NIR absorption spectroscopy. The continuous irradiation led to the reduction of the $BIPY^{2+}$ units, giving rise to two new absorption bands centered on 400 and 605 nm, characteristic absorptions[68] of $BIPY^{(\bullet+)}$ radical cations. After irradiation for ~100 min, the absorption intensity reached (Figure 7c) a maximum, indicating that the reduction was complete. When irradiation was halted and the sample was exposed to air, the changes of absorption spectra were reversed (Figure 7b). In other words, the absorption bands centered on both 400 and 605 nm decreased and eventually the original spectrum was restored after ~50 min.

Encouraged by this success in the case of **Ru^{2+}-Box^{4+}**, we carried out the photoreduction on **Ru^{2+}-Cat^{6+}** under the same conditions. The spectra (Figure 7d) for **Ru^{2+}-Cat^{6+}** display absorption features similar to those for **Ru^{2+}-Box^{4+}** with two

DOI: 10.1021/acs.jpca.5b04570
J. Phys. Chem. A XXXX, XXX, XXX−XXX

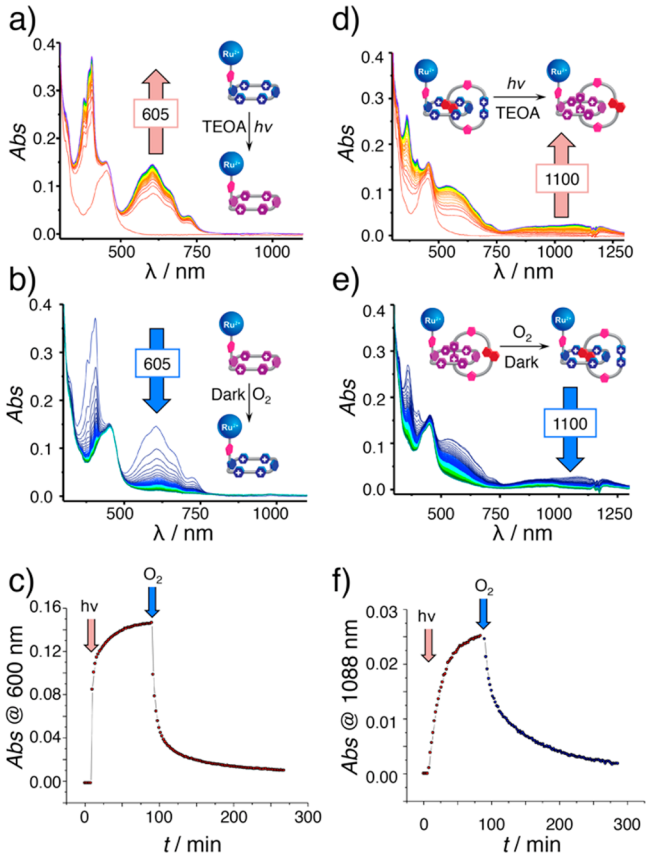

Figure 7. Steady-state UV–vis–NIR absorption spectra of solutions (MeCN, 298 K, argon, 10 μM) containing (a, b) **Ru^{2+}-Box^{4+}** and (d, e) **Ru^{2+}-Cat^{6+}** in the presence of an excess of TEOA irradiated with a laser source (λ_{exc} = 450 nm) and subsequently oxidized by introducing air. Plots of absorbance against the irradiation time and oxidation time of (c) **Ru^{2+}-Box^{4+}** at 600 nm and (f) **Ru^{2+}-Cat^{6+}** at 1088 nm.

absorption bands—namely, MLCT and LC—in relation to the Ru(bpy)$_3^{2+}$ unit. Noticeably, the weak donor–acceptor CT band (λ_{max} ~ 520 nm, ε ~ 700 M^{-1} cm^{-1}) associated with the DNP ⊂ CBPQT^{4+} co-conformation is masked by the much stronger MLCT band of the Ru(bpy)$_3^{2+}$ unit in the same region. Irradiation of a deaerated MeCN solution led to the emergence of a broad absorption band centered on 1100 nm, accompanied by another absorption band centered on 530 nm. The appearance of these two characteristic absorption bands supports[63] the formation of the trisradical co-conformation. Along with the CV studies, these results indicate that the CBPQT$^{2(\bullet+)}$ ring moves from the DNP to the BIPY$^{(\bullet+)}$ recognition site upon photoreduction. After ~100 min of irradiation, the photoreduction and switching process were complete. By exposing the irradiated solution to air in the dark, the absorption bands corresponding to the trisradical co-conformation slowly disappeared over a course of a little more than 100 min and the initial absorption spectrum (Figure 7e) was restored, an observation that demonstrates that the CBPQT^{4+} ring encircles the DNP unit once again. To this end, we achieved switching the CBPQT^{4+} ring between two different recognition sites by sequential irradiation and oxidation. In addition to the laser source, we demonstrate that a household visible-light lamp, without any light filter, can also trigger the switching. The UV–vis–NIR spectra recorded for a household-lamp irradiated sample demonstrate (Figure S12, Supporting Information) that 1 h of irradiation is also sufficient to complete the switch over.

Additionally, a qualitative analysis (Figure 7c,f) of the time to oxidize **Ru^{2+}-Box$^{2(\bullet+)}$** and **Ru^{2+}-Cat$^{3(\bullet+)}$** suggests that **Ru^{2+}-Box$^{2(\bullet+)}$** is easier oxidized than **Ru^{2+}-Cat$^{3(\bullet+)}$**. This observation can be rationalized by the fact that, in the case of **Ru^{2+}-Cat$^{3(\bullet+)}$**, the oxidation requires breaking favorable radical–radical interactions, a situation that consumes more energy to overcome barriers associated with the mechanical movements.

The photoreduced states of both **Ru^{2+}-Box^{4+}** and **Ru^{2+}-Cat^{6+}** were probed (Figure 8) by EPR spectroscopy. Both irradiated solutions of **Ru^{2+}-Box^{4+}** and **Ru^{2+}-Cat^{6+}** in the presence of TEOA are EPR active, indicating the successful photoreduction of BIPY^{2+} units. The EPR spectrum of **Ru^{2+}-Box$^{2(\bullet+)}$** displays a broad hyperfine splitting compared with that of methyl viologen,[79] suggesting that its two BIPY$^{(\bullet+)}$ units exist in an intermediate spin–spin exchange interaction regime. The EPR spectrum of **Ru^{2+}-Cat$^{3(\bullet+)}$** exhibits an even broader hyperfine splitting as a consequence of an intermolecular spin–spin exchange interaction between the CBPQT$^{2(\bullet+)}$ ring and the BIPY$^{(\bullet+)}$ unit.

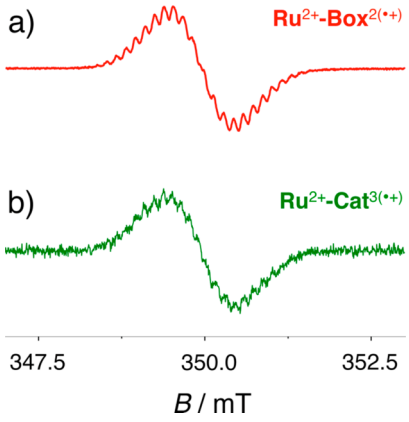

Figure 8. EPR spectra of solutions (MeCN, 298 K, argon, 100 μM) containing (a) **Ru^{2+}-Box^{4+}** and (b) **Ru^{2+}-Cat^{6+}** in an excess of TEOA after being irradiated for 60 min.

Besides the evidence for the switching process obtained from UV–vis–NIR and EPR spectroscopies, the photoreduction of **Ru^{2+}-Cat^{6+}** in CD$_3$CN was also examined by ^{1}H NMR spectroscopy. Prior to exposing to visible light, the ^{1}H NMR spectrum (Figure 9a) recorded at room temperature for a CD$_3$CN solution containing **Ru^{2+}-Cat^{6+}** and an excess of TEOA reveals a broad doublet at 6.3 ppm and a broad singlet at 6.05 ppm, arising from the H$_{2/6}$ and H$_{3/7}$ protons, respectively, on the DNP unit, an observation that indicates the CBPQT^{4+} ring encircles the DNP unit. After being degassed for 10 min, the sample was irradiated with a household lamp for 1 h, during which time the sample color turned from orange to deep purple. The ^{1}H NMR spectrum (Figure 9b) of the irradiated sample reveals that proton resonances associated with the encircled DNP unit disappeared, indicating the formation of the BIPY$^{(\bullet+)}$ radical cations. After air was purged for another 1 min, the color of the solution reverted to orange and the DNP proton resonances in the ^{1}H NMR spectrum (Figure S13, Supporting Information) were restored, suggesting that the CBPQT^{4+} ring had moved back onto the DNP unit. Because the switching cycles were repeated five times (Figures 9c and S13, Supporting Information) and no significant decomposition

DOI: 10.1021/acs.jpca.5b04570
J. Phys. Chem. A XXXX, XXX, XXX–XXX

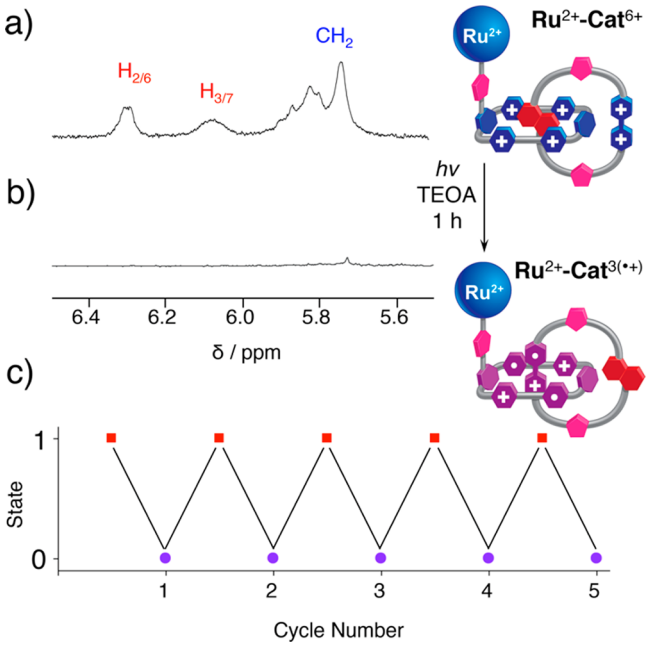

Figure 9. Partial ^{1}H NMR spectra (500 MHz, CD_3CN, 298 K) of (a) **Ru^{2+}-Cat^{6+}** and (b) after being irradiated for 60 min with a household lamp in an excess of TEOA. (c) Plot of switching states upon visible light irradiation and oxidation versus cycle number monitored by using ^{1}H NMR spectroscopy. "1" denotes the state where the $CBPQT^{4+}$ ring encircles the DNP unit and "0" denotes the state where the $CBPQT^{2(\bullet+)}$ ring encircles the $BIPY^{(\bullet+)}$ unit.

was observed, this photoactive bistable [2]catenane shows considerable promise as a robust artificial molecular switch.

CONCLUSION

We have synthesized and characterized a novel visible light-driven switchable [2]catenane. By employing VT ^{1}H NMR spectroscopy, two dynamic processes—that is, (i) the rotations of both the $BIPY^{2+}$ units and the phenylene groups and (ii) the disassociation and recombination of the DNP unit—in association with the photoactive [2]catenane were identified, and their activation free energies were calculated to be 16.1 and 14.4 kcal mol^{-1}, respectively at 298 K. We have also demonstrated, by employing UV−vis−NIR, ^{1}H NMR and EPR spectroscopies, that visible light irradiation can reduce the $BIPY^{2+}$ dications to $BIPY^{(\bullet+)}$ radical cations, triggering the switching of the $CBPQT^{2(\bullet+)}$ ring from the DNP to the $BIPY^{(\bullet+)}$ recognition site. Oxidation by introducing air reinstates the $CBPQT^{4+}$ ring onto the DNP unit. This switch, which provides a primitive example of mimicking biological molecular motors by employing very simple external stimuli, serves as a source inspiration in building more complex switches.

ASSOCIATED CONTENT

Supporting Information

Full details of instrumentation and analytical techniques; synthesis and characterization data for **Ru^{2+}-Box^{4+}** and **Ru^{2+}-Cat^{6+}**; VT ^{1}H NMR study for the complex **3** ⊂ **Ru^{2+}-Box^{4+}**; dynamics of **Ru^{2+}-Box^{6+}** and **Ru^{2+}-Cat^{6+}**; fsTA of **1^{2+}**, **Ru^{2+}-Box^{6+}**, and **Ru^{2+}-Cat^{6+}**; UV−vis−NIR investigation of photoreduction of **Ru^{2+}-Cat^{6+}** using a household lamp; ^{1}H NMR investigation on visible light-driven switching cycles of **Ru^{2+}-Cat^{6+}**. The Supporting Information is available free of charge on the ACS Publications website at DOI: 10.1021/acs.jpca.5b04570.

AUTHOR INFORMATION

Corresponding Authors

*M. R. Wasielewski. E-mail: m-wasielewski@northwestern.edu.
*J. F. Stoddart. E-mail: stoddart@northwestern.edu.

Notes

The authors declare no competing financial interest.

ACKNOWLEDGMENTS

We thank Drs. Zhixue Zhu and Hao Li for helpful discussions and Dr. Ryan Young for assistance with fsTA measurements. This research is part (Project 34-949) of the Joint Center of Excellence in Integrated Nano-Systems (JCIN) at King Abdulaziz City for Science and Technology (KACST) and Northwestern University (NU) and also supported by a grant from the US National Science Foundation (CHE-1266201) (M.R.W.). The authors thank both KACST and NU for their continued support of this research. Y.W. thanks the International Institute for Nanotechnology (IIN) at NU for the award of a Ryan Fellowship and the Fulbright Scholar Program for a Reserach Fellowship. D.C. who was the recipient of a Graduate Research Fellowship from the National Science Foundation also gratefully acknowledges support from a Ryan Fellowship awarded by the NU IIN.

REFERENCES

(1) Vale, R. D. The Molecular Motor Toolbox for Intracellular Transport. *Cell* **2003**, *112*, 467−480.
(2) Boyer, P. D. The Binding Change Mechanism for ATP Synthase—Some Probabilities and Possibilities. *Biochim. Biophys. Acta, Bioenerg.* **1993**, *1140*, 215−250.
(3) Abrahams, J. P.; Leslie, A. G. W.; Lutter, R.; Walker, J. E. Structure at 2.8 Å Resolution of F1-ATPase from Bovine Heart Mitochondria. *Nature* **1994**, *370*, 621−628.
(4) Boyer, P. D. The ATP Synthase-A Splendid Molecular Machine. *Annu. Rev. Biochem.* **1997**, *66*, 717.
(5) Kinosita, K., Jr. F1-ATPase: A Prototypical Rotary Molecular Motor. *Adv. Exp. Med. Biol.* **2012**, *726*, 5−16.
(6) Finer, J. T.; Simmons, R. M.; Spudich, J. A. Single Myosin Molecule Mechanics: Piconewton Forces and Nanometre Steps. *Nature* **1994**, *368*, 113−119.
(7) Holmes, K. C. The Swinging Lever-arm Hypothesis of Muscle Contraction. *Curr. Biol.* **1997**, *7*, R112−118.
(8) Jon Kull, F.; Sablin, E. P.; Lau, R.; Fletterick, R. J.; Vale, R. D. Crystal Structure of the Kinesin Motor Domain Reveals a Structural Similarity to Myosin. *Nature* **1996**, *380*, 550−555.
(9) Ryu, W. S.; Berry, R. M.; Berg, H. C. Torque-Generating Units of the Flagellar Motor of Escherichia Coli Have a High Duty Ratio. *Nature* **2000**, *403*, 444−447.
(10) Balzani, V.; Credi, A.; Raymo, F. M.; Stoddart, J. F. Artificial Molecular Machines. *Angew. Chem., Int. Ed.* **2000**, *39*, 3348−3391.
(11) Collin, J.-P.; Dietrich-Buchecker, C.; Gaviña, P.; Jimenez-Molero, M. C.; Sauvage, J.-P. Shuttles and Muscles: Linear Molecular Machines Based on Transition Metals. *Acc. Chem. Res.* **2001**, *34*, 477−487.
(12) Harada, A. Cyclodextrin-Based Molecular Machines. *Acc. Chem. Res.* **2001**, *34*, 456−464.
(13) Kinbara, K.; Aida, T. Toward Intelligent Molecular Machines: Directed Motions of Biological and Artificial Molecules and Assemblies. *Chem. Rev.* **2005**, *105*, 1377−1400.
(14) Sauvage, J.-P. Transition Metal-Complexed Catenanes and Rotaxanes as Molecular Machine Prototypes. *Chem. Commun.* **2005**, 1507−1510.

DOI: 10.1021/acs.jpca.5b04570
J. Phys. Chem. A XXXX, XXX, XXX−XXX

(15) Feringa, B. L. The Art of Building Small: From Molecular Switches to Molecular Motors. *J. Org. Chem.* **2007**, *72*, 6635−6652.
(16) Kay, E. R.; Leigh, D. A.; Zerbetto, F. Synthetic Molecular Motors and Mechanical Machines. *Angew. Chem., Int. Ed.* **2007**, *46*, 72−191.
(17) Saha, S.; Stoddart, J. F. Photo-Driven Molecular Devices. *Chem. Soc. Rev.* **2007**, *36*, 77−92.
(18) Michl, J.; Sykes, E. C. H. Molecular Rotors and Motors: Recent Advances and Future Challenges. *ACS Nano* **2009**, *3*, 1042−1048.
(19) Vogelsberg, C. S.; Garcia-Garibay, M. A. Crystalline Molecular Machines: Function, Phase Order, Dimensionality, and Composition. *Chem. Soc. Rev.* **2012**, *41*, 1892−1910.
(20) van Dongen, S. F. M.; Cantekin, S.; Elemans, J. A. A. W.; Rowan, A. E.; Nolte, R. J. M. Functional Interlocked Systems. *Chem. Soc. Rev.* **2014**, *43*, 99−122.
(21) Schill, G. *Catenanes, Rotaxanes, and Knots*; Academic Press: New York, 1971.
(22) Amabilino, D. B.; Stoddart, J. F. Interlocked and Intertwined Structures and Superstructures. *Chem. Rev.* **1995**, *95*, 2725−2828.
(23) Breault, G. A.; Hunter, C. A.; Mayers, P. C. Supramolecular Topology. *Tetrahedron* **1999**, *55*, 5265−5293.
(24) *Molecular Catenanes, Rotaxanes and Knots: A Journey Through the World of Molecular Topology*; Sauvage, J. P., Dietrich-Buchecker, C., Eds.; Wiley-VCH: Weinheim, 1999.
(25) Crowley, J. D.; Goldup, S. M.; Lee, A.-L.; Leigh, D. A.; McBurney, R. T. Active Metal Template Synthesis of Rotaxanes, Catenanes and Molecular Shuttles. *Chem. Soc. Rev.* **2009**, *38*, 1530−1541.
(26) Stoddart, J. F. The Chemistry of the Mechanical Bond. *Chem. Soc. Rev.* **2009**, *38*, 1802−1820.
(27) Fang, L.; Olson, M. A.; Benitez, D.; Tkatchouk, E.; Goddard, W. A., III; Stoddart, J. F. Mechanically Bonded Macromolecules. *Chem. Soc. Rev.* **2010**, *39*, 17−29.
(28) Beves, J. E.; Blight, B. A.; Campbell, C. J.; Leigh, D. A.; McBurney, R. T. Strategies and Tactics for the Metal-Directed Synthesis of Rotaxanes, Knots, Catenanes, and Higher Order Links. *Angew. Chem., Int. Ed.* **2011**, *50*, 9260−9327.
(29) Neal, E. A.; Goldup, S. M. Chemical Consequences of Mechanical Bonding in Catenanes and Rotaxanes: Isomerism, Modification, Catalysis and Molecular Machines for Synthesis. *Chem. Commun.* **2014**, *50*, 5128−5142.
(30) Troisi, A.; Ratner, M. A. Conformational Molecular Rectifiers. *Nano Lett.* **2004**, *4*, 591−595.
(31) Green, J. E.; Choi, J. W.; Boukai, A.; Bunimovich, Y.; Johnston-Halperin, E.; DeIonno, E.; Luo, Y.; Sheriff, B. A.; Xu, K.; Shik Shin, Y.; Tseng, H.-R.; et al. A 160-Kilobit Molecular Electronic Memory Patterned at 10^{11} Bits per Square Centimetre. *Nature* **2007**, *445*, 414−417.
(32) Heath, J. R. Molecular Electronics. *Annu. Rev. Mater. Res.* **2009**, *39*, 1−23.
(33) van der Molen, S. J.; Peter, L. Charge Transport through Molecular Switches. *J. Phys.: Condens. Matter* **2010**, *22*, 133001.
(34) Jia, C.; Li, H.; Jiang, J.; Wang, J.; Chen, H.; Cao, D.; Stoddart, J. F.; Guo, X. Interface-Engineered Bistable [2]Rotaxane-Graphene Hybrids with Logic Capabilities. *Adv. Mater.* **2013**, *25*, 6752−6759.
(35) Angelos, S.; Khashab, N. M.; Yang, Y.-W.; Trabolsi, A.; Khatib, H. A.; Stoddart, J. F.; Zink, J. I. pH Clock-Operated Mechanized Nanoparticles. *J. Am. Chem. Soc.* **2009**, *131*, 12912−12914.
(36) Tarn, D.; Ferris, D. P.; Barnes, J. C.; Ambrogio, M. W.; Stoddart, J. F.; Zink, J. I. A Reversible Light-Operated Nanovalve on Mesoporous Silica Nanoparticles. *Nanoscale* **2014**, *6*, 3335−3343.
(37) Monnereau, C.; Ramos, P. H.; Deutman, A. B. C.; Elemans, J. A. A. W.; Nolte, R. J. M.; Rowan, A. E. Porphyrin Macrocyclic Catalysts for the Processive Oxidation of Polymer Substrates. *J. Am. Chem. Soc.* **2010**, *132*, 1529−1531.
(38) Wang, J.; Feringa, B. L. Dynamic Control of Chiral Space in a Catalytic Asymmetric Reaction Using a Molecular Motor. *Science* **2011**, *331*, 1429−1432.
(39) Blanco, V.; Carlone, A.; Hänni, K. D.; Leigh, D. A.; Lewandowski, B. A Rotaxane-Based Switchable Organocatalyst. *Angew. Chem., Int. Ed.* **2012**, *51*, 5166−5169.
(40) Lewandowski, B.; De Bo, G.; Ward, J. W.; Papmeyer, M.; Kuschel, S.; Aldegunde, M. J.; Gramlich, P. M. E.; Heckmann, D.; Goldup, S. M.; D'Souza, D. M.; et al. Sequence-Specific Peptide Synthesis by an Artificial Small-Molecule Machine. *Science* **2013**, *339*, 189−193.
(41) Blanco, V.; Leigh, D. A.; Marcos, V.; Morales-Serna, J. A.; Nussbaumer, A. L. A Switchable [2]Rotaxane Asymmetric Organocatalyst That Utilizes an Acyclic Chiral Secondary Amine. *J. Am. Chem. Soc.* **2014**, *136*, 4905−4908.
(42) van Dongen, S. F. M.; Elemans, J. A. A. W.; Rowan, A. E.; Nolte, R. J. M. Processive Catalysis. *Angew. Chem., Int. Ed.* **2014**, *53*, 11420−11428.
(43) Clavel, C.; Romuald, C.; Brabet, E.; Coutrot, F. A pH-Sensitive Lasso-Based Rotaxane Molecular Switch. *Chem. Eur. J.* **2013**, *19*, 2982−2989.
(44) Grunder, S.; McGrier, P. L.; Whalley, A. C.; Boyle, M. M.; Stern, C.; Stoddart, J. F. A Water-Soluble pH-Triggered Molecular Switch. *J. Am. Chem. Soc.* **2013**, *135*, 17691−17694.
(45) Lu, T.-W.; Chang, C.-F.; Lai, C.-C.; Chiu, S.-H. Molecular Switch Based on Very Weak Association between BPX26C6 and Two Recognition Units. *Org. Lett.* **2013**, *15*, 5742−5745.
(46) Beves, J. E.; Blanco, V.; Blight, B. A.; Carrillo, R.; D'Souza, D. M.; Howgego, D.; Leigh, D. A.; Slawin, A. M. Z.; Symes, M. D. Toward Metal Complexes That Can Directionally Walk Along Tracks: Controlled Stepping of a Molecular Biped with a Palladium(II) Foot. *J. Am. Chem. Soc.* **2014**, *136*, 2094−2100.
(47) Raehm, L.; Kern, J.-M.; Sauvage, J.-P. A Transition Metal Containing Rotaxane in Motion: Electrochemically Induced Pirouetting of the Ring on the Threaded Dumbbell. *Chem. Eur. J.* **1999**, *5*, 3310−3317.
(48) Andersen, S. S.; Share, A. I.; Poulsen, B. L. C.; Kørner, M.; Duedal, T.; Benson, C. R.; Hansen, S. W.; Jeppesen, J. O.; Flood, A. H. Mechanistic Evaluation of Motion in Redox-Driven Rotaxanes Reveals Longer Linkers Hasten Forward Escapes and Hinder Backward Translations. *J. Am. Chem. Soc.* **2014**, *136*, 6373−6384.
(49) Bruns, C. J.; Frasconi, M.; Iehl, J.; Hartlieb, K. J.; Schneebeli, S. T.; Cheng, C.; Stupp, S. I.; Stoddart, J. F. Redox Switchable Daisy Chain Rotaxanes Driven by Radical−Radical Interactions. *J. Am. Chem. Soc.* **2014**, *136*, 4714−4723.
(50) Livoreil, A.; Sauvage, J.-P.; Armaroli, N.; Balzani, V.; Flamigni, L.; Ventura, B. Electrochemically and Photochemically Driven Ring Motions in a Disymmetrical Copper [2]-Catenate. *J. Am. Chem. Soc.* **1997**, *119*, 12114−12124.
(51) Brouwer, A. M.; Frochot, C.; Gatti, F. G.; Leigh, D. A.; Mottier, L.; Paolucci, F.; Roffia, S.; Wurpel, G. W. H. Photoinduction of Fast, Reversible Translational Motion in a Hydrogen-Bonded Molecular Shuttle. *Science* **2001**, *291*, 2124−2128.
(52) Leigh, D. A.; Wong, J. K. Y.; Dehez, F.; Zerbetto, F. Unidirectional Rotation in a Mechanically Interlocked Molecular Rotor. *Nature* **2003**, *424*, 174−179.
(53) Mobian, P.; Kern, J.-M.; Sauvage, J.-P. Light-Driven Machine Prototypes Based on Dissociative Excited States: Photoinduced Decoordination and Thermal Recoordination of a Ring in a Ruthenium(II)-Containing [2]Catenane. *Angew. Chem., Int. Ed.* **2004**, *43*, 2392−2395.
(54) Balzani, V.; Clemente-León, M.; Credi, A.; Ferrer, B.; Venturi, M.; Flood, A. H.; Stoddart, J. F. Autonomous Artificial Nanomotor Powered by Sunlight. *Proc. Natl. Acad. Sci. U. S. A.* **2006**, *103*, 1178−1183.
(55) Raiteri, P.; Bussi, G.; Cucinotta, C. S.; Credi, A.; Stoddart, J. F.; Parrinello, M. Unravelling the Shuttling Mechanism in a Photoswitchable Multicomponent Bistable Rotaxane. *Angew. Chem., Int. Ed.* **2008**, *47*, 3536−3539.
(56) Li, H.; Fahrenbach, A. C.; Coskun, A.; Zhu, Z.; Barin, G.; Zhao, Y.-L.; Botros, Y. Y.; Sauvage, J.-P.; Stoddart, J. F. A Light-Stimulated

DOI: 10.1021/acs.jpca.5b04570
J. Phys. Chem. A XXXX, XXX, XXX−XXX

Molecular Switch Driven by Radical−Radical Interactions in Water. *Angew. Chem., Int. Ed.* **2011**, *50*, 6782−6788.
(57) Avellini, T.; Li, H.; Coskun, A.; Barin, G.; Trabolsi, A.; Basuray, A. N.; Dey, S. K.; Credi, A.; Silvi, S.; Stoddart, J. F.; et al. Photoinduced Memory Effect in a Redox Controllable Bistable Mechanical Molecular Switch. *Angew. Chem., Int. Ed.* **2012**, *51*, 1611−1615.
(58) Zhu, Z.; Fahrenbach, A. C.; Li, H.; Barnes, J. C.; Liu, Z.; Dyar, S. M.; Zhang, H.; Lei, J.; Carmieli, R.; Sarjeant, A. A.; et al. Controlling Switching in Bistable [2]Catenanes by Combining Donor−Acceptor and Radical−Radical Interactions. *J. Am. Chem. Soc.* **2012**, *134*, 11709−11720.
(59) Bruns, C. J.; Fujita, D.; Hoshino, M.; Sato, S.; Stoddart, J. F.; Fujita, M. Emergent Ion-Gated Binding of Cationic Host−Guest Complexes within Cationic $M_{12}L_{24}$ Molecular Flasks. *J. Am. Chem. Soc.* **2014**, *136*, 12027−12034.
(60) Kosower, E. M.; Cotter, J. L. Stable Free Radicals. II. The Reduction of 1-Methyl-4-cyanopyridinium Ion to Methylviologen Cation Radical. *J. Am. Chem. Soc.* **1964**, *86*, 5524−5527.
(61) Jeon, W. S.; Ziganshina, A. Y.; Lee, J. W.; Ko, Y. H.; Kang, J.-K.; Lee, C.; Kim, K. A [2]Pseudorotaxane-Based Molecular Machine: Reversible Formation of a Molecular Loop Driven by Electrochemical and Photochemical Stimuli. *Angew. Chem., Int. Ed.* **2003**, *42*, 4097−4100.
(62) Trabolsi, A.; Khashab, N.; Fahrenbach, A. C.; Friedman, D. C.; Colvin, M. T.; Cotí, K. K.; Benítez, D.; Tkatchouk, E.; Olsen, J.-C.; Belowich, M. E.; et al. Radically Enhanced Molecular Recognition. *Nat. Chem.* **2010**, *2*, 42−49.
(63) Fahrenbach, A. C.; Barnes, J. C.; Lanfranchi, D. A.; Li, H.; Coskun, A.; Gassensmith, J. J.; Liu, Z.; Benítez, D.; Trabolsi, A.; Goddard, W. A., III; et al. Solution-Phase Mechanistic Study and Solid-State Structure of a Tris(bipyridinium radical cation) Inclusion Complex. *J. Am. Chem. Soc.* **2012**, *134*, 3061−3072.
(64) Liu, F.; Concepcion, J. J.; Jurss, J. W.; Cardolaccia, T.; Templeton, J. L.; Meyer, T. J. Mechanisms of Water Oxidation from the Blue Dimer to Photosystem II. *Inorg. Chem.* **2008**, *47*, 1727−1752.
(65) Gagliardi, C. J.; Vannucci, A. K.; Concepcion, J. J.; Chen, Z.; Meyer, T. J. The Role of Proton Coupled Electron Transfer in Water Oxidation. *Energy Environ. Sci.* **2012**, *5*, 7704−7717.
(66) Prier, C. K.; Rankic, D. A.; MacMillan, D. W. C. Visible Light Photoredox Catalysis with Transition Metal Complexes: Applications in Organic Synthesis. *Chem. Rev.* **2013**, *113*, 5322−5363.
(67) Thompson, D. W.; Ito, A.; Meyer, T. J. $[Ru(bpy)_3]^{2+*}$ and other remarkable metal-to-ligand charge transfer (MLCT) excited states. *Pure Appl. Chem.* **2013**, *85*, 1257−1305.
(68) Ma, D.; Bettis, S. E.; Hanson, K.; Minakova, M.; Alibabaei, L.; Fondrie, W.; Ryan, D. M.; Papoian, G. A.; Meyer, T. J.; Waters, M. L.; et al. Interfacial Energy Conversion in Ru^{II} Polypyridyl-Derivatized Oligoproline Assemblies on TiO_2. *J. Am. Chem. Soc.* **2013**, *135*, 5250−5253.
(69) Olson, M. A.; Coskun, A.; Klajn, R.; Fang, L.; Dey, S. K.; Browne, K. P.; Grzybowski, B. A.; Stoddart, J. F. Assembly of Polygonal Nanoparticle Clusters Directed by Reversible Noncovalent Bonding Interactions. *Nano Lett.* **2009**, *9*, 3185−3190.
(70) Wang, C.; Cao, D.; Fahrenbach, A. C.; Grunder, S.; Dey, S. K.; Sarjeant, A. A.; Stoddart, J. F. The Effects of Conformation on the Noncovalent Bonding Interactions in a Bistable Donor−Acceptor [3]Catenane. *Chem. Commun.* **2012**, *48*, 9245−9247.
(71) Spruell, J. M.; Paxton, W. F.; Olsen, J.-C.; Benítez, D.; Tkatchouk, E.; Stern, C. L.; Trabolsi, A.; Friedman, D. C.; Goddard, W. A., III.; Stoddart, J. F. A Push-Button Molecular Switch. *J. Am. Chem. Soc.* **2009**, *131*, 11571−11580.
(72) Sutherland, I. O. The Investigation of the Kinetics of Conformational Changes by Nuclear Magnetic Resonance Spectroscopy. *Annu. Rep. NMR Spectrosc.* **1971**, *4*, 71−235.
(73) The plot of $\ln(k/T)$ against $1/T$ gives a straight line. $\Delta H^{\ddagger}$ and $\Delta S^{\ddagger}$ can be calculated from slope and intercept in the Eyring plot of $\ln(k/T) = -\Delta H^{\ddagger}/RT + \ln(k_B/h) + \Delta S^{\ddagger}/R$.
(74) The line-shape analyses were carried out by using the NUMMRIT simulation module incorporated in the software SpinWorks 2.5.5, which can be downloaded from ftp://davinci.chem.umanitoba.ca/pub/marat/SpinWorks.
(75) Innocenzi, P.; Kozuka, H.; Yoko, T. Fluorescence Properties of the $Ru(bpy)_3^{2+}$ Complex Incorporated in Sol-Gel-Derived Silica Coating Films. *J. Phys. Chem. B* **1997**, *101*, 2285−2291.
(76) Caspar, J. V.; Meyer, T. J. Photochemistry of $Ru(bpy)_3^{2+}$. Solvent Effects. *J. Am. Chem. Soc.* **1983**, *105*, 5583−5590.
(77) Yonemoto, E. H.; Saupe, G. B.; Schmehl, R. H.; Hubig, S. M.; Riley, R. L.; Iverson, B. L.; Mallouk, T. E. Electron-Transfer Reactions of Ruthenium Trisbipyridyl−Viologen Donor−Acceptor Molecules: Comparison of the Distance Dependence of Electron Transfer-Rates in the Normal and Marcus Inverted Regions. *J. Am. Chem. Soc.* **1994**, *116*, 4786−4795.
(78) Kirch, M.; Lehn, J.-M.; Sauvage, J.-P. Hydrogen Generation by Visible Light Irradiation of Aqueous Solutions of Metal Complexes. An Approach to the Photochemical Conversion and Storage of Solar Energy. *Helv. Chim. Acta* **1979**, *62*, 1345−1384.
(79) Benniston, A. C.; Harriman, A.; Li, P.; Rostron, J. P.; Harrington, R. W.; Clegg, W. A Spectroscopic Study of the Reduction of Geometrically Restrained Viologens. *Chem. Eur. J.* **2007**, *13*, 7838−7851.

DOI: 10.1021/acs.jpca.5b04570
J. Phys. Chem. A XXXX, XXX, XXX−XXX